CONTENTS

MNRAS **000**, 000–000 (0000) Preprint 13 September 2021 Compiled using MNRAS LATEX style file v3.0

Architecture of Planetary Systems in Mean Motion Resonance

JT Laune,[1] Laetitia Rodet,[1] and Dong Lai[1]
[1]*Department of Astronomy and Space Sciences, Cornell University*

1 INTRODUCTION

The typical outcome of planet-disk migration is thought to be capture into mean motion resonance, after which torques from the gas damp the system's angular momentum deficit (AMD) into equilibrium. The MMR equilibrium is governed by various conditions which are well studied in the literature (e.g. (Henrard and Lemaitre, 1983; Deck and Batygin, 2015; Goldreich and Schlichting, 2014; Xu et al., 2018; Henrard and Lemaitre, 1983))

2 PLANET MIGRATION

Planets embedded within a protoplanetary disk interact gravitationally with the gas and lose angular momentum, leading to inward migration towards the central star. Disk torques vary with planet mass as well as across semimajor axis; large outer planets lose angular momentum quickly and sweep up inner planets into MMRs (Tanaka and Ward, 2004; Xu et al., 2018). In some cases, the planet can gain angular momentum and migrate away from the primary.

In this paper, we will ignore the detailed physics of planet-disk interactions and instead implement dissipative forces parametrized by the eccentricity damping and migration timescales, denoted by $T_{e,i}$ and $T_{m,i}$ for $i = 1, 2$. The accelerations are then given by:

$$\frac{\dot{e}_i}{e_i} = -\frac{1}{T_{e,i}} \tag{1}$$

$$\frac{\dot{a}_i}{a_i} = -\frac{1}{T_{m,i}} - \frac{2e_i^2}{T_{e,i}}. \tag{2}$$

In our notation, $T_{m,i} > 0$ (< 0) denotes inward (outward) migration. For typical, flat disk profiles, we have (Tanaka and Ward, 2004; Cresswell and Nelson, 2008; Xu et al., 2018)

$$\frac{T_{e,1}}{T_{e,2}} = \frac{1}{q} \tag{3}$$

$$T_{e,i} = 3.46h^2 T_{m,i}. \tag{4}$$

To scale the dissipation times in the integrations, we choose a parameter $T_{e,0}$ and set

$$T_{e,1} = T_{e,0}\sqrt{q} \tag{5}$$

$$T_{e,2} = T_{e,0}/\sqrt{q}. \tag{6}$$

We must have $1/T_{m,1} - 1/T_{m,2} > 0$ for convergent (i.e. $|a_1 - a_2|$ is shrinking) inward migration, and vice versa for outward migration. Hence, for $q > 1$, we set $T_{m,i} < 0$; for $q < 1$, we set $T_{m,i} > 0$. Unless noted otherwise, we choose $h = 0.1$ and $T_{e,0} = 1000$ years . We'll refer to these relationships as the "standard picture" of planet migration.

2.1 MMR

When two planets have commensurate period ratios, $p : q$ where p, q are integers, their gravitational interactions may lock them into a mean motion resonance (MMR). As young planets migrate within their disk, if the migration is convergent (i.e. P_2/P_1 decreasing), they cross MMR period ratios and may be captured. In our paper, we will be considering only first order MMRs, denoted by $j : j + 1$, which occur where $n_2/n_1 = j/j + 1$, where n_1, n_2 denote the inner and outer planet, respectively.

The Hamiltonian of a system with two planets near a first order MMR is (Murray and Dermott, 2000):

$$\begin{aligned} H_{\rm kep} &= -\frac{GMm_1}{2a_1} - \frac{GMm_2}{2a_2} \\ H_{\rm res} &= -\frac{Gm_1m_2}{a_2}\left[f_1 e_1 \cos\theta_1 + f_2 e_2 \cos\theta_2\right] \\ H_{\rm sec} &= -\frac{Gm_1m_2}{a_2}\left[f_3(e_1^2 + e_2^2) + f_4 e_1 e_2 \cos(\varpi_2 - \varpi_1)\right] \\ H &= H_{\rm kep} + H_{\rm res} + H_{\rm sec}. \end{aligned} \tag{7}$$

$H_{\rm kep}$ is the standard Keplerian Hamiltonian; $H_{\rm res}$ the resonant interactions between the planets of order $\mathcal{O}(e_i)$; and $H_{\rm sec}$ the secular interactions. The two angles are given by

$$\theta_i = (j+1)\lambda_2 - \lambda_1 - \varpi_i. \tag{8}$$

Equation (7) admits eight coupled ODES $(\dot{a}_i, \dot{e}_i, \dot{\theta}_i, \dot{\varpi}_i)$, which we may integrate together with the effects of dissipation to simulate MMR capture. An example of MMR capture is given in Figure 1. The period ratio P_2/P_1 initially starts wide of the nominal resonance value of 1.5. After around 2 kyr of convergent migration, the planets are caught into MMR, indicated by the stabilization of θ_1 to 180° and θ_2 to 0°. The planets' eccentricities level off at around 4 kyr near $e_1 \approx 0.02$ and $e_2 \approx 0.04$, and the planets become apsidally anti-aligned with $\varpi_1 - \varpi_2 \approx 180°$.

In this paper, we will use the term "resonance" loosely to mean the libration of an angle such as θ_1, θ_2, and later on $\hat{\theta}$. We'll also use the angle itself to refer to the resonance, i.e. the planets m_1 and m_2 in Figure 1 are caught into both θ_1 and θ_2, respectively, since those angles are librating.

During the migration phase, planets typically retain small eccentricities. Indeed, the standard circular MMRs (angles θ_1 and θ_2) have finite resonance widths in e, and so small

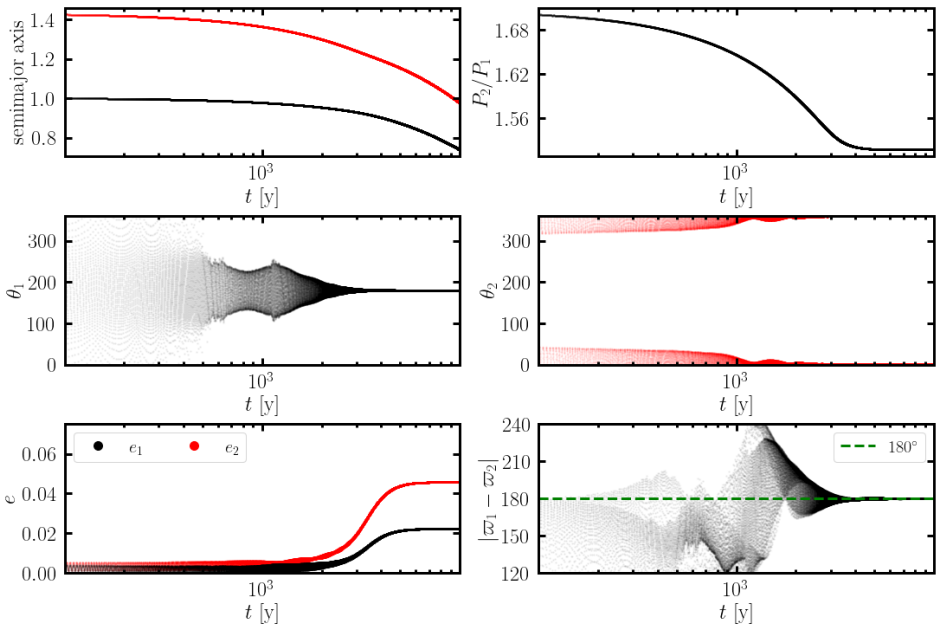

Figure 1. Standard MMR capture process for $h = 0.1$ and $q = 2$. The outer planet m_2 starts wide of resonance and is captured near $t = 2000$ yrs, after which the two angles $\theta_1 \to 180°$ and $\theta_2 \to 0°$. While in resonance, the e_i values are driven to equilibrium and the periapses are antialigned.

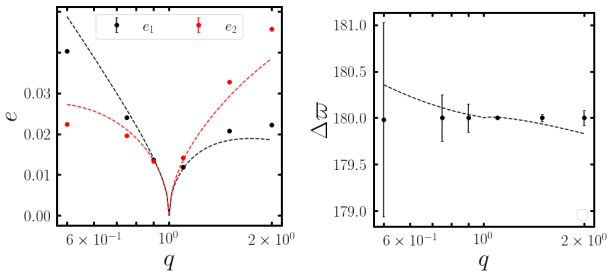

(a) (b)

Figure 2. *(a)* Analytical equilibrium values are plotted as dashed lines for various values of q. The points indicate time averaged numerical results from integrating the time-dependent equations of motion. Error bars indicate the standard deviation of the eccentricities; most fall within the marker for eccentricity. Simulations without secular effects showed only negligible differences, and so they were not included. *(b)* Same as *(a)*, but for $\Delta\varpi$. Simulations without secular effects did show significant differences, and so they have been included.

eccentricities are necessary for capture. Most studies consider only the resonant terms for this reason, since they are first order in eccentricity. However, if eccentricities are excited, secular terms play an important role, and so we keep them.

2.2 Equilibrium

The MMR capture in Figure 1 reaches an equilibrium state in period ratio, resonant angles, eccentricities, and $\Delta\varpi$. Indeed, the Hamiltonian in equation (7), including the dissipative terms, admits the following three equations for equilibrium values of $(e_1, e_2, \theta_1, \theta_2)$:

$$\dot{e}_1 = \frac{\mu_2}{\alpha_2}[f_1 \sin(\theta_1) - De_2 \sin(\gamma_2 - \gamma_1)] - \frac{e_1}{T_{e,1}} = 0 \qquad (9)$$

$$\dot{e}_2 = \frac{q\mu_2}{\alpha_2}[f_2 \sin(\theta_2) - De_1 \sin(\gamma_1 - \gamma_2)] - \frac{e_2}{T_{e,2}} = 0 \qquad (10)$$

$$\frac{d}{dt}\Delta\varpi \equiv \dot{\varpi}_1 - \dot{\varpi}_2 = \frac{\mu_2}{\alpha_2}\left[\frac{f_1 \cos\theta_1}{\alpha_1^{1/2} e_1} - \frac{q f_2 \cos\theta_2}{\alpha_2^{1/2} e_2} + \frac{2C}{\alpha_1^{1/2}} + \frac{De_2}{\alpha_1^{1/2} e_1} - \frac{2qC}{\alpha_2^{1/2}} - \frac{qDe_1}{\alpha_2^{1/2} e_2}\right] = 0 \qquad (11)$$

where we have combined $\Delta\varpi = \theta_2 - \theta_1 = \varpi_1 - \varpi_2$ in the last equation.

We must find a fourth equation to complete this system of equations. Absent any dissipative forces, the following quantities are conserved:

$$J = \Lambda_1\sqrt{1 - e_1^2} + \Lambda_2\sqrt{1 - e_2^2} \qquad (12)$$

$$G = \frac{j+1}{j}\Lambda_1 + \Lambda_2. \qquad (13)$$

The quantity J is the angular momentum of the system, and G is an integral of motion for equation (7).

Define η to be a clever combination of J and G,

$$\eta(\alpha, e_1, e_2) \equiv -2(q/\alpha_0 + 1)\left(\frac{J}{G} - \left.\frac{J}{G}\right|_0\right), \qquad (14)$$

(15)

where $\alpha_0 = (j/(j+1))^{3/2}$ and $(J/G|_0$ is evaluated at $e_i = 0$ and $\alpha = \alpha_0$. Thus, we have $\eta(\alpha_0, 0, 0) = 0$ and the corresponding Taylor expansion yields

$$\eta \approx -\frac{q(\alpha - \alpha_0)}{j\sqrt{\alpha_0}(q/\alpha_0 + 1)} + q\sqrt{\alpha_0}e_1^2 + e_2^2 \qquad (16)$$

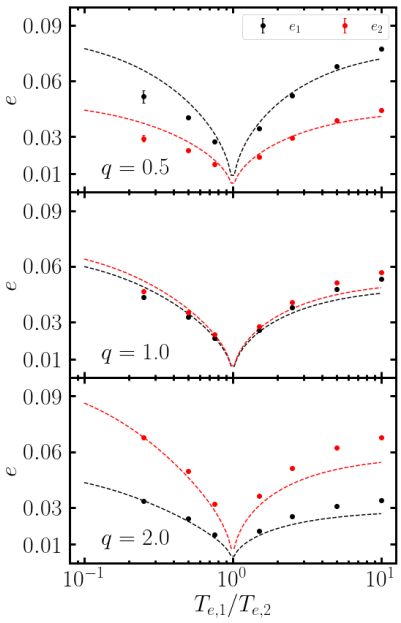

Figure 3. Equilibrium eccentricity values for a range of $T_{e,1}/T_{e,2} \in [0.2, 10]$ are plotted for three different values of $q = 0.5, 1.0$, and 2.0. The points and errorbars are calculated in the same way as 2. The dashed lines indicate analytical estimates for e_i.

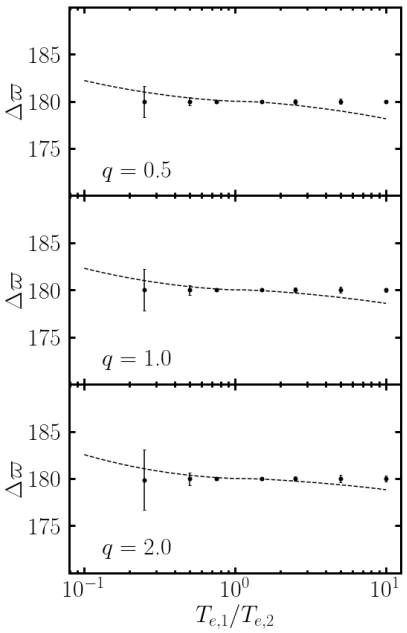

Figure 4. Same as 3 but for $\Delta\varpi$.

The equation of motion for η is then given by

$$\dot{\eta} = \frac{q\alpha_0^{1/2}}{j(q\alpha_0^{-1}+1)}\left[\frac{1}{T_{m2}} - \frac{1}{T_{m1}} + \frac{2e_1^2}{T_{e1}} - \frac{2e_2^2}{T_{e2}}\right] - q\alpha_0^{1/2}\frac{2e_1^2}{T_{e1}} - \frac{2e_2^2}{T_{e2}} = 0. \quad (17)$$

We note that the only contribution to $\dot{\eta}$ is from dissipative effects.

By solving the four equations (9) – (11) and (17) , we may arrive at equilibrium values for the system. In the standard picture and neglecting secular terms (i.e., for small e_i), equations (9) and (10) show $\sin(\theta_i) \approx 0$. Equation (11) then gives us $\theta_1 \approx \pi$ and $\theta_2 \approx 0$. Since $\theta_1 - \theta_2 = \varpi_2 - \varpi_1$, we therefore see that convergent migration produces anti-aligned periapses. We confirm this in the time-dependent integration in Figure 1. The equilibrium e_i's and $\Delta\varpi$'s for comparable mass planets ($q \in [0.5, 2]$) are given in Figures 2a and 2b. Analytical results are plotted as dashed lines. Here we also integrate the time-dependent differential equations from Hamiltonian (7) and plot the average e_1, e_2, and $\Delta\varpi$ over the last 10\calculated with outward migration for $q > 1$ and inward migration for $q < 1$.

As we can see, the final averaged eccentricities for m_1 and m_2 go approximately as $e_1/e_2 \sim q$. As expected, the $\Delta\varpi$ average values are all very close to π. The numerical and analytical results largely agree.

In the next two sections, we will explore slightly modified models by varying the ratio $T_{e,1}/T_{e,2}$ within $[0.1q, 10q]$.

2.3 Eccentricity damping timescales

Up until now, we have strictly been considering the standard picture of planet migration– with $T_{e,1}/T_{e,2} = 1/q$ and $\$T_{e,i}=3.46h^{2}T_{e,i}\$$– which always gives rise to apsidal anti-alignment for reasonable values of h. This simple parametrized model will always fail to capture all of the complicated hydrodynamics of real astrophysical disks. We can therefore easily expect a difference in the ratio $T_{e,1}/T_{e,2}$ over an order of magnitude, and perhaps this modfication could produce $\Delta\varpi \approx 0°$ without adding new parameters to the system.

We explore this possibility in Figures 3 and 4. The ratio $T_{e,1}/T_{e,2}$ varies freely between 0.2 and 10, regardless of the mass ratio. Initially, we attempted to extend this range to $T_{e,1}/T_{e,2} = 0.1$, but the system eventually escapes resonance for all $q=0.5,$ 1, and 2 and no equilibrium is reached. The migration timescales are set to $|T_{m,i}| = T_{e,i}/3.46h^2$. For $T_{e,1} < T_{e,2}$, then, we set $T_{m,i} > 0$, corresponding to outward migration, and vice versa for $T_{e,1} > T_{e,2}$.

For comparable mass planets with $q = 0.5$, 1, and 2, varying the ratio $T_{e,1}/T_{e,2}$ around $1/q$ modifies the final equilibrium eccentricities by a roughly similar factor, as seen in Figure 3. The eccentricity ratio e_1/e_2 is largely unchanged, yet the magnitudes e_1 and e_2 are larger for more extreme values of $T_{e,1}/T_{e,2}$. The dashed lines plot the analytic results from solving equations (9) – (17); these findings reproduce the numerical results.

The corresponding values for $\Delta\varpi$ are shown in 4; variations in the eccentricity damping ratio cannot account for apsidal alignment. In all cases, the analytic equilibrium equations predict $\Delta\varpi \approx 180°$, and the numerical integrations agree.

3 APSIDAL ALIGNMENT

As we have seen, capture into the θ_1 and θ_2 resonance always leads to $\Delta\varpi = 180°$ due to their equilibrium values being 180° and 0°, respectively. The apsidally anti-aligned K2-19 system therefore poses a problem for our standard model. In

order to match this observation, either θ_1, θ_2, or both angles must cease to be in resonance.

3.1 Eccentricity driving forces

One way of escaping the circular θ_i resonances is to artificially drive the eccentricity of the system to larger values, where θ_i will cease to act. We modify the eccentricity damping for m_2 in (1) to be

$$\frac{\dot{e}_2}{e_2} = -\frac{(e_2 - e_{2,d})}{T_{e,2d}}. \tag{18}$$

Hence, planet m_2 is exponentially driven to $e_{2,d}$ with a timescale of $T_{e,2}$. In principle, this could be done for both e_1 and e_2, but we restrict our study to e_2 for simplicity.

In Figure 5, we demonstrate the feasibility of this approach, where we have added in the driving force with $e_{2,d} = 0.3$ by hand and set $q = 2$. We initalize the system close to resonance, where it stays for around 8,000 years. Between $t = 8,000$ and $10,000$ years, e_1 and e_2 grow and the system subsequently breaks out of both the θ_1 and θ_2 resonances. At this point, both planets' ecentricities are excited to about $e_i \approx 0.2$ and the planets become apsidally aligned as $\Delta\varpi$ librates around 0° with an amplitde of around 100°.

3.2 Large initial eccentricities

Another way of avoiding capture into the circular θ_i resonances altogether is to have a large initial eccentricity when the periods P_2/P_1 reach the nominal resonance value of 1.5. In Figure 6 , we demonstrate the feasibility of MMR apsidal-alignment when the planets m_1 and m_2 are given large initial eccentricities of $e_1 = e_2 = 0.2$ by hand at the start of the integration.

One weakness of this scenario is that the dissipative forces must be shut off at some point after the system is captured into resonance but before it evolves to a true equilibrium. If the disk forces were left on for the entire simulation, the planets would reach the standard equilibrium and "forget" their initial conditions. Because of this, we chose to set $T_{w,0} = 10$ kyr rather than the standard 1 kyr. This requires some fine tuning, but it is within the realm of possibility as the protoplanetary disk does indeed dissipate over time. Depending on other system parameters, the disk could indeed disappear before the system reaches equilibrium, at which point the resonance would cease to evolve.

3.3 Reducing the Hamiltonian

A detailed analysis of the MMR Hamiltonian (7) illustrates the underlying dynamics behind the capture processes in Figures 6 and 8 which lead to apsidal alignment.

Following (Henrard et al., 1986) (or equivalently (Wisdom, 1986)), we may transform the Hamiltonian $H_{\rm Kep} + H_{\rm res}$ in equation (7) into the form

$$\hat{H}(R, \hat{\theta}) = -3(\delta + 1)R + R^2 - 2\sqrt{2R}\cos(\hat{\theta}) \tag{19}$$

through a series of rotations in phase space. Consider the phase space configuration $\boldsymbol{\xi} = (\theta_1, \theta_2, \Gamma_1, \Gamma_2)$, where the Γ_i are the Poincairé momenta $\Gamma_i = \Lambda_i(1 - \sqrt{1 - e_i^2})$. Let $\boldsymbol{X}$ be the cartesian formulation

$$\begin{aligned}\boldsymbol{X} &= (x_1, x_2, X_1, X_2) \\ &= (\sqrt{2\Gamma_1}\cos\theta_1, \sqrt{2\Gamma_2}\cos\theta_2, \sqrt{2\Gamma_1}\sin\theta_1, \sqrt{2\Gamma_2}\sin\theta_2)\end{aligned} \tag{20}$$

The resonant Hamiltonian becomes

$$H_{\rm res} \propto f_1 x_1 + f_2 x_2$$

Let $\boldsymbol{\Psi}$ be the counter-clockwise rotation by angle ψ defined by $\tan\psi = f_1/f_2$:

$$\boldsymbol{\Psi} = \frac{1}{f_2\sqrt{f_1^2 + f_2^2}}\begin{pmatrix} f_2 & f_1 \\ -f_1 & f_2 \end{pmatrix}. \tag{21}$$

The block matrix

$$\boldsymbol{M} = \begin{pmatrix} \boldsymbol{\Psi} & \boldsymbol{0} \\ \boldsymbol{0} & \boldsymbol{\Psi} \end{pmatrix} \tag{22}$$

is symplectic (Goldstein et al., 2000). The Laplace coefficients f_i depend weakly on the semimajor axis ratio α, and so $\boldsymbol{M}$ only represents a canonical transformation if α is stationary or varying adiabatically, which is a good approximation for the systems considered in this paper.

Define the coordinates

$$\boldsymbol{W} = \boldsymbol{M}\boldsymbol{X}. \tag{23}$$

Somewhat

The canonical coordinate $\hat{\theta}$ is given by the equation

$$\tan\left(\pi - \hat{\theta}\right) = \frac{e_1\sin(\theta_1) + (f_2/f_1)e_2\sin(\theta_2)}{e_1\cos(\theta_1) + (f_2/f_1)e_2\cos(\theta_2)}, \tag{24}$$

where we have included a shift by π so that $\hat{\theta}$ has an equilibrium value at 0 rather than π.

We define $\hat{\boldsymbol{e}} = |f_1|\boldsymbol{e}_1 - |f_2|\boldsymbol{e}_2$ so that the conjugate momentum R is

$$R \propto ||\hat{\boldsymbol{e}}||^2 = f_1^2 e_1^2 - 2|f_1 f_2|e_1 e_2\cos(\varpi_1 - \varpi_2) + f_2^2 e_2^2 \tag{25}$$

where $\boldsymbol{e}_i$ is the Runge-Lenz vector, i.e. the vector with magnitude e_i in the direction of perihelion. The true value includes total scaling factors such as $\mu_{\rm tot}$. For our purposes, $\hat{\boldsymbol{e}}$ will suffice.

For the case $e_1 = 0$ and $\mu_2 \ll \mu_1$, the system's conjugate momentum takes the form $R \sim e_1^2$ with coordinate $\hat{\theta} = \theta_1$, and vice versa for $e_2 = 0$, $\mu_1 \ll \mu_2$. These parameters describe the standard scenario of a test particle near an MMR with a massive planet on a circular orbit, the derivation of which may be found in (Murray and Dermott, 2000). The parameter δ describes the system's depth into resonance.

Since the canonical momenta of the circular angles θ_i have $R_i \propto e_i^2$, resonance capture widths δa_i are functions of e_i as well. Hence, for large eccentricities near the resonance location, m_1 and m_2 may not be captured into resonance. However, if we consider the Hamiltonian system $H_{\rm Kep} + H_{\rm res}$ in (7) as a whole, i.e. considering m_1 and m_2 simultaneously, there is one resonance angle $\hat{\theta}$ that describes the system's dynamics which may operate separately from θ_1 and θ_2.

The resonant equation of motion for R is

$$\dot{R}_{\rm res} = -\frac{\partial\hat{H}}{\partial\hat{\theta}} = -2\sqrt{2R}\sin(\hat{\theta}) = 0 \tag{26}$$

in resonance. Hence, only dissipative and secular forces are

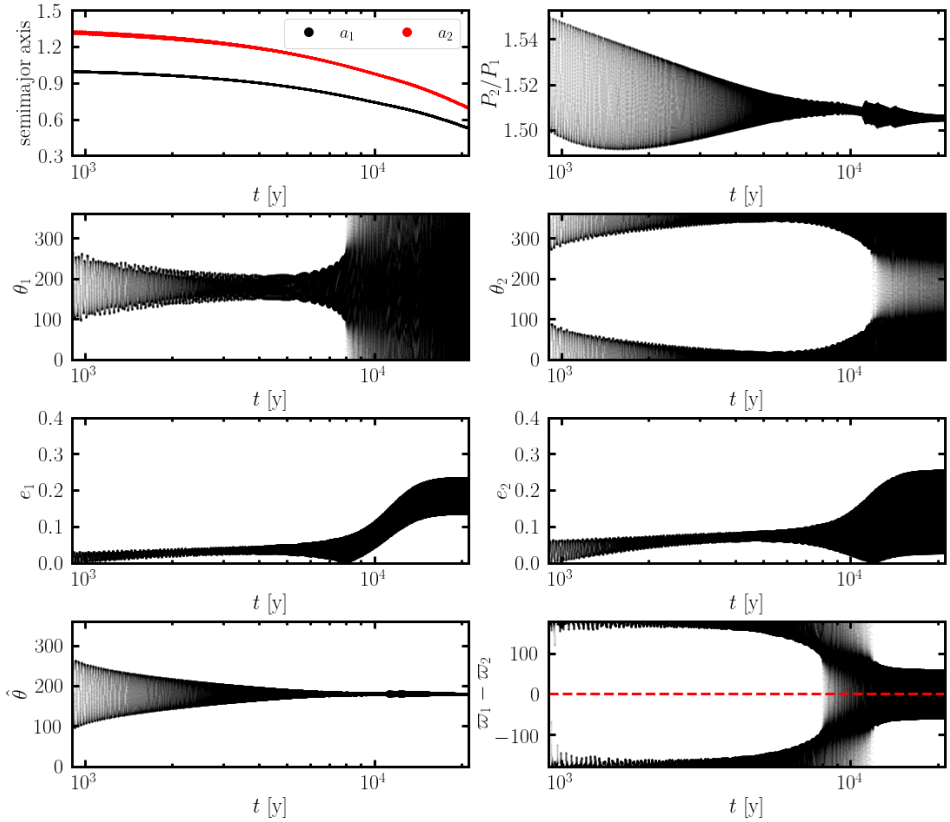

Figure 5. Here we have set $e_{2,d} = 0.3$ with $h = 0.1$ and $q = 2$. After about 10 kyr, the system escapes the circular resonances and becomes apsidally aligned.

at play if $\hat{\theta}$ is operating. The integrations in Figures 5 and 6 do not show qualitative differences if the secular terms are turned off, and so the apsidal alignment must be due to dissipation. If we assume the semimajor axis ratio is constant and consider only the dissipative effects on R, we arrive at the following relation for equilibrium in R:

$$\cos \Delta\varpi \sim \frac{e_1^2 T_{e,2} + e_2^2 T_{e,1}}{e_1 e_2 (T_{e,1} + T_{e,2})}. \tag{27}$$

For reasonable disk parameters ($h \sim 0.1$, $T_{e,i} \sim h^2 T_{m,i}$), the right hand side of equation (27) is order unity, and so we see that $\Delta\varpi \approx 0$.

The Hamiltonian in (19) is known as "the second fundamental model of resonance". Its phase space is well studied in the literature, so we will only review it briefly, following the approach in (Henrard and Lemaitre, 1983). The choice of polar coordinates in equation (24) introduces a virtual singularity at $R = 0$ (Henrard and Lemaitre, 1983). If we switch to the canonical Cartesian coordinates $\xi = \sqrt{R}\cos\theta$ and $\nu = \sqrt{R}\cos\theta$, $\hat{H}$ becomes

$$\hat{H}(\xi, \nu) = -3(\delta + 1)(\xi^2 + \nu^2) + (\xi^2 + \nu^2)^2 - 2\sqrt{2}\xi \tag{28}$$

In equilibrium, $\dot{R} = \partial\hat{H}/\partial\theta \propto \sin\theta = 0$, and so we see that equilibria must lie along the line $\nu = 0$ in phase space. The left panel of Figure 7 displays the results of solving the equation $\hat{H}(\xi, 0) = 0$ for ξ numerically for various values of δ. For $\delta < 0$, there is one equilibrium point to the right of the origin; for $\delta \geq 0$, a separatrix appears which divides the phase space into 3 regions: outer circulation (outside the separatrix), inner circulation (within the inner lobe of the separatrix), and the resonance zone (between the inner and outer lobe of the separatrix). The resonance zone is indicated in red in the left panel of Figure 7. The right two panels of Figure 7 display the phase space for choices of positive and negative δ.

3.4 Phase space paths

In 8, we display the phase spaces from all three integrations plotted in the previous sections. The top row displays the $(\theta_2, \propto e_2)$ conjugate pair. The standard setup enters a tight resonance quickly and stays there (indicated by the small yellow region). Driving e_2 to a value $e_{2,d} = 0.3$ leads to an early libration, indicated by the blue-green inner lobe. The planet m_2 then enters the outer circulation region and reaches equilibrium. On the contrary, the simulation with both $e_1 = e_2 = 0.2$ starts well outside the separatrix (purple). Dissipative forces push the system closer to the separatrix; then, the disk forces cease and the system remains in the circulation region. This way, the system never enters the θ_2 resonance. The θ_1 resonance is similar.

On the other hand, the bottom row of 8 displays the phase space for $(\hat{\theta}, \propto \hat{e})$. All three systems end up in resonance. The standard picture is a very tight resonance, while the e_2 -driving and large e_0 systems enter stable libration in the resonance zone. The two apsidally aligned cases therefore end

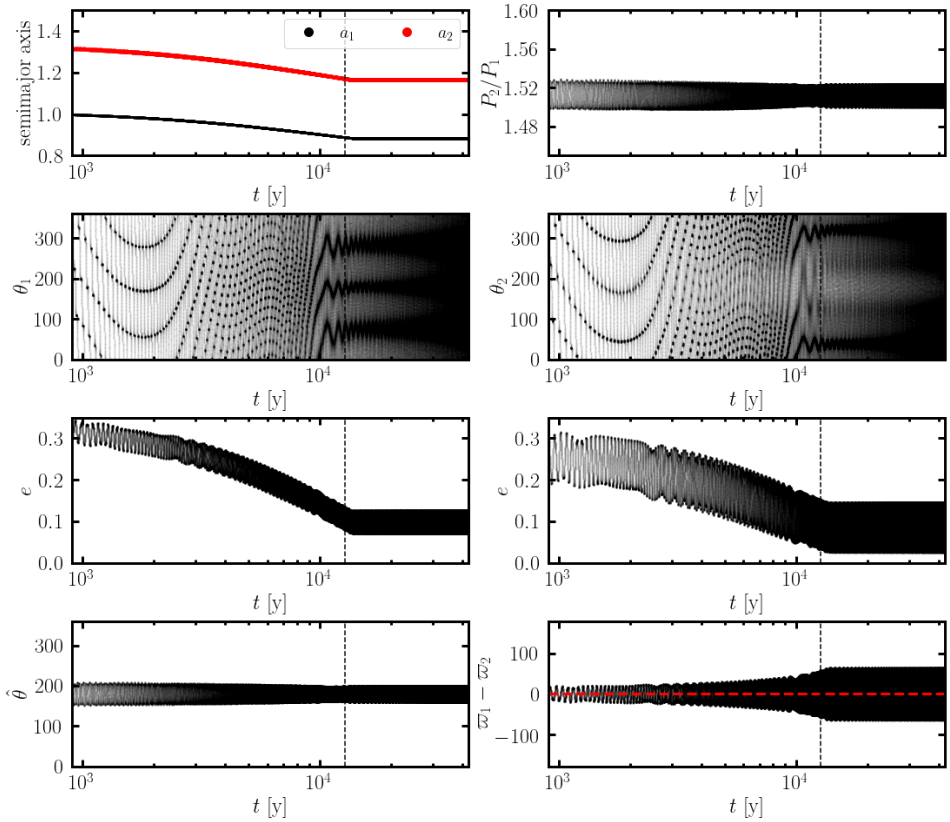

Figure 6. Here we again have an example with $h = 0.1$, $q = 2$, but set the initial eccentricities to $e_{i,0} = 0.3$ and $T_{e,0} = 10$ kyr. The system misses the circular resonances altogether and remains apsidally aligned throughout.

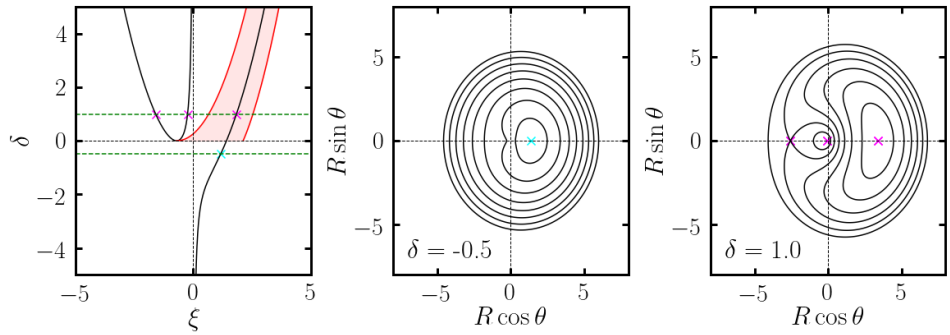

Figure 7. *Left*: Equilibrium points for the Hamiltonian in equation (19) for various values of δ are plotted in black. The green lines indicate the δ values used for the right two phase diagrams, along with their associated equilibria. The resonance zone for $\delta > 0$ is shaded in red. *Middle*: Phase diagram for $\delta = -0.5$. There is only a single equilibrium and resonance zone to the right of the origin. *Right*: Phase diagram for $\delta = 1$. There are three equilibria; the separatrix passes through the leftmost equilibrium point, which is a saddle point in phase space. The small lobe of the separatrix encloses a circulation zone with a stable equilibrium near the origin. The leftmost equilibrium point is located within the resonance zone in between the two lobes of the separatrix.

up in analagous phase space configurations, but through different dynamical paths.

4 CONCLUSION

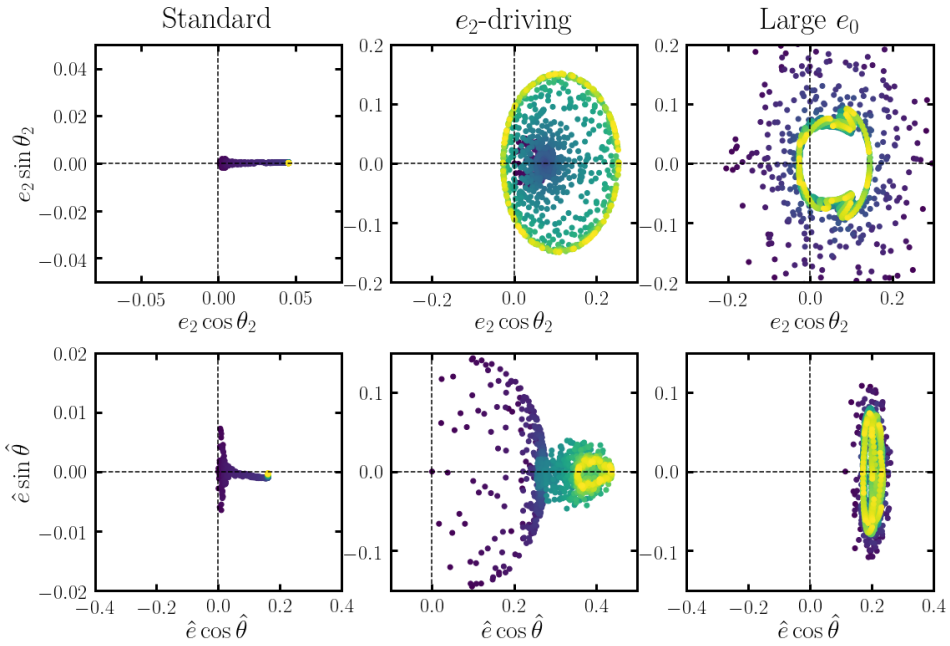

Figure 8. Here we have plotted each example runs' path through phase space. On the top row, we plot only the $e_2 \longleftrightarrow \theta_2$ resonance to save space; the $e_1 \longleftrightarrow \theta_1$ resonance is similar. Time is indicated by color, with purple near $t = 0$ and yellow near the end of the simulation. All times are scaled to the beginning and end times of the integration for comparison, not physical time. *Left:* The standard example. Here we see both the θ_2 and $\hat{\theta}$ resonances are acting. *Middle:* The case with eccentricity driving forces. The system starts near the origin in (e_2, θ_2) space, and moves outwards to the circulation zone due to the driving forces. *Right:* Similar to the driving force case, but this time the system starts well outside of the resonance zone in (e_2, θ_2) space and then gets trapped into the circulation zone due to dissipative forces.

5 APPENDIX

5.1 Elliptic restricted 3 body problem

REFERENCES

Cresswell, P. and Nelson, R. P. (2008). Three-dimensional simulations of multiple protoplanets embedded in a protostellar disc. *Astronomy & Astrophysics*, 482(2):677–690.

Deck, K. M. and Batygin, K. (2015). Migration of two massive planets into (and out of) first order mean motion resonances. *The Astrophysical Journal*, 810(2):119. arXiv: 1506.01382.

Goldreich, P. and Schlichting, H. E. (2014). Overstable Librations can Account for the Paucity of Mean Motion Resonances among Exoplanet Pairs. *The Astronomical Journal*, 147:32.

Goldstein, Poole, and Sako (2000). *Classical Mechanics*. 3rd edition.

Henrard, J. and Lemaitre, A. (1983). A second fundamental model for resonance. *Celestial mechanics*, 30(2):197–218.

Henrard, J., Lemaitre, A., Milani, A., and Murray, C. D. (1986). The reducing transformation and apocentric librators. *Celestial Mechanics*, 38(4):335–344.

Murray, C. D. and Dermott, S. F. (2000). *Solar System Dynamics*. Cambridge University Press, Cambridge.

Tanaka, H. and Ward, W. R. (2004). Three-dimensional Interaction between a Planet and an Isothermal Gaseous Disk. II. Eccentricity Waves and Bending Waves. *The Astrophysical Journal*, 602(1):388.

Wisdom, J. (1986). Canonical solution of the two critical argument problem. *Celestial Mechanics*, 38:175–180.

Xu, W., Lai, D., and Morbidelli, A. (2018). Migration of Planets Into and Out of Mean Motion Resonances in Protoplanetary Discs: Overstability of Capture and Nonlinear Eccentricity Damping. *Monthly Notices of the Royal Astronomical Society*, 481(2):1538–1549. arXiv: 1805.07501.